The development of short pitch rail corrugation

Extensive field monitoring and validation of numerical predictions

Zhang, Pan; Li, Zili

DOI
10.1016/j.triboint.2025.110821

Publication date
2025

Document Version
Final published version

Published in
Tribology International

Tribology International 210 (2025) 110821

Contents lists available at ScienceDirect

Tribology International

journal homepage: www.elsevier.com/locate/triboint

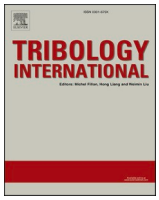

The development of short pitch rail corrugation: Extensive field monitoring and validation of numerical predictions

Pan Zhang, Zili Li *

Delft University of Technology, Section of Railway Engineering, Stevinweg 1, Delft 2628 CN, the Netherlands

ARTICLE INFO

Keywords:
Short pitch rail corrugation
Field validation
Initiation and consistent growth
Longitudinal vibrations

ABSTRACT

Short pitch corrugation is a major rail defect worldwide, and its development mechanism remains not fully understood. This work aims to better understand corrugation and validate some numerical predictions through extensive field monitoring. 105 corrugations on four sections of mainline tracks were continually monitored for five years. Comprehensive field data were collected, including photos, geometry, and vehicle-track dynamic responses. Numerical results of corrugation development agree with the field observations. It confirms that corrugation initiates with necessary initial excitation, consistently grows at fixed locations due to differential wear, and eventually reaches a limiting amplitude. Moreover, vehicle-track longitudinal vibrations are crucial to corrugation initiation, while vertical vibration plays an increasingly important role in corrugation growth.

1. Introduction

Rail transportation plays a significant role in reducing carbon emissions. Many countries are planning to greatly expand their railway networks as part of efforts to achieve carbon-neutral transport. However, the presence of defects makes rail transport less appealing and competitive, hindering its application and development. Short pitch corrugation, a major defect extensively found on various types of railway lines such as mainlines [1], metros [2], high-speed lines [3] and continuously-supported rail lines [4], is particularly problematic. Short pitch corrugation (hereafter corrugation) is (quasi-) periodical uneven wear on the rail surface on straight tracks or gentle curves with wavelengths typically falling in 20–80 mm [5], often visually recognized as dark and bright patterns (Fig. 1a). The undulant surface of corrugation generates high levels of noise and vibration during train passage [6,7], which is annoying and detrimental to passengers and residents near the railway lines. Moreover, corrugation excites large wheel-rail dynamic force [8], induces rolling contact fatigue (RCF) cracks [9] (Fig. 1b), and accelerates the deterioration of vehicle-track components [10–12]. Maintenance cost has to be greatly increased to not only treat corrugations but also its adverse consequences [4]. Therefore, it is important to develop effective solutions to eliminate or mitigate corrugation, based on a thorough understanding of the formation mechanism.

Corrugation development is a complex long-term process determined by vehicle-track dynamic interactions and the resulting rail material damage [13]. Despite extensive research efforts and various hypotheses proposed in the literature, the corrugation mechanism has not been fully understood, and corrugation remains a severe problem in the global railway networks. Vehicle-track dynamic interactions are essentially three-dimensional (3D) in the vertical, longitudinal (rolling) and lateral directions [14–16]. Most researchers assumed that the vehicle-track vertical interaction excited by initial rail roughness determines corrugation formation at single or multiple resonance modes, such as pinned-pinned [17,18], rail resonance [19] and sleeper anti-resonance modes [20,21]. Moreover, it is suggested that vertical rail bending modes within the bogie distance may also induce corrugation [22–24]. The hypotheses based on vertical resonance modes can predict the corrugation occurrence at some locations, but have difficulty explaining the corrugation-free tracks observed in the field. Some researchers suggested that corrugation could develop due to vehicle-track lateral dynamic interaction, for instance, at lateral 1st and 2nd pinned-pinned modes [25,26] or by frictional unstable vibrations [1,27]. Nevertheless, on tangent tracks where corrugations mainly occur [5], the lateral dynamic interaction with a small yaw angle is usually insignificant, which seems unlikely to cause consistent corrugation growth.

Few researchers investigated the influence of vehicle-track longitudinal dynamic interaction on corrugation formation, as the longitudinal force is typically assumed to be a constant or dependent on the vertical (normal) dynamic force [28]. However, numerical results in [29] indicate that the characteristic frequencies of the longitudinal dynamic force

* Corresponding author.
E-mail address: z.li@tudelft.nl (Z. Li).

https://doi.org/10.1016/j.triboint.2025.110821
Received 3 January 2025; Received in revised form 17 May 2025; Accepted 19 May 2025
Available online 20 May 2025

can differ from those of the vertical force, depending on the longitudinal track dynamics. Furthermore, it is reported in [30] that the longitudinal dynamic force considerably exceeds the vertical force within the frequency range of 200–1500 Hz, given equal amplitudes of relative displacement. These simulation results align with field axle box acceleration (ABA) measurements, which show that the longitudinal ABA signals contain different frequency components from the vertical ABA, with much stronger vibration magnitudes and energy at light squats or indentations [31].

In light of the findings in [29–31], a series of studies [32–37] have been performed to better understand the corrugation development, with an emphasis on vehicle-track longitudinal dynamic interaction. In these studies, an advanced 3D finite element (FE) vehicle-track interaction model [38] and an innovative downscale V-Track test rig [39] have been employed. Compared to the other models [40–42] and testing facilities [43–45], the 3D FE model and the V-Track have the advantage of simultaneously and accurately simulating the 3D high-frequency dynamics and wheel-rail frictional rolling contact of the real vehicle-track system [46–49], which are essential to corrugation formation. Numerical simulations in [32–34,36] reveal that rail longitudinal vibration modes, rather than the commonly considered vertical modes, are dominant for corrugation initiation. It is also predicted that rail corrugation consistently grows at a fixed location with the continuous accumulation of differential wear. These findings have been verified by two corrugation experiments using the V-Track test rig [35,37].

This work is subsequent to the numerical simulations and laboratory experiments in [32–37], aiming to provide field validation for the proposed corrugation mechanism. This validation work is based on five years of continual monitoring data at 105 corrugations on four types of railway tracks. Unlike other field observations [1,50], this study not only recorded corrugation photos and geometry, but also obtained the track dynamic behaviours and the vehicle-track dynamic responses. With these more comprehensive field data, the development of corrugation can be better understood. Besides, this work could serve as a reference for evaluating various theories of corrugation formation. The structure of this paper is organized as follows. 2 introduces the field conditions and monitoring method of rail corrugation. 3 validates the numerical predictions of corrugation development. 4 presents more corrugation features observed in the field. 5 discusses the evolution of rail roughness and the role of vertical pinned-pinned resonance in corrugation formation. The main conclusions are summarized in 6.

2. Field monitoring of rail corrugation

This section first introduces the field conditions of the monitored tracks for investigation of rail corrugation, such as their locations, major track components and traffic characteristics. Afterwards, the monitoring method is described in detail, including photographing, rail geometry measurement, track dynamics testing, and axle box accelerations (ABA) measurement.

2.1. Field conditions

Four sections of straight tracks were selected in the Dutch railway networks for five-year continual monitoring, from September 2007 (2007.09) to November 2012 (2012.11), as shown in Fig. 2. These four monitored tracks all had one-directional traffic with the majority being passenger trains. They were ballasted tracks using the nominal rail profile UIC54E1, made from R260Mn steel. The sleeper spacing was 0.6 m, and the vertical fastening stiffness was about 800–1300 MN/m, estimated from the measured frequency response functions (FRFs).

Track 1 (Fig. 2a) was located in Steenwijk, the Netherlands, connecting a curved track and the Steenwijk station. It utilized the Deenik fastenings and bi-block concrete sleepers. The train speed was about 130 km/h after exiting the curve and some traction was needed to maintain this speed. The annual traffic load was around 3.4 million gross tonnages (MGT). Track 2 (Fig. 2b) was situated in Assen following a curve and used the W-shaped tension clips and bi-block concrete sleepers. The nominal traffic speed was 140 km/h and the annual load was approximately 6.3 MGT. Track 3 (Fig. 2c) was situated in Weert followed by a curve. This track consisted of W-shaped fastenings and monoblock concrete sleepers. Trains run on this section of track with a constant speed of about 140 km/h and would brake before entering the curve. The annual traffic was about 3.0 MGT. Track 4 (Fig. 2d) was located in Wirdum just before a curve. The rails were fixed on wooden sleepers with W-shaped fastenings. Trains operated at a maximum speed of 140 km/h on this track, and its annual traffic load was about 4.2 MGT. This information has been summarized in Table 1.

It can be seen that the selected four sections of straight tracks were located either after or before curved tracks so that certain traction or braking force was expected at the wheel-rail interface, creating a potentially favourable condition for corrugation formation [35]. Moreover, these four tracks were chosen with different track components (i.e., sleepers and fastenings), enabling us to examine whether the numerical predictions in [32,33,36] are generally applicable across various track configurations.

105 locations were monitored on these four sections of tracks for investigating corrugation. Specifically, 50 sites were on Track 1, 30 on Track 2, 15 on Track 3, and 10 on Track 4. Each site was labelled with a unique number (e.g., TU101 in Fig. 2a) and its position was marked on the rail side by a short yellow line. Their GPS positions were also recorded for alignment with the ABA measurement.

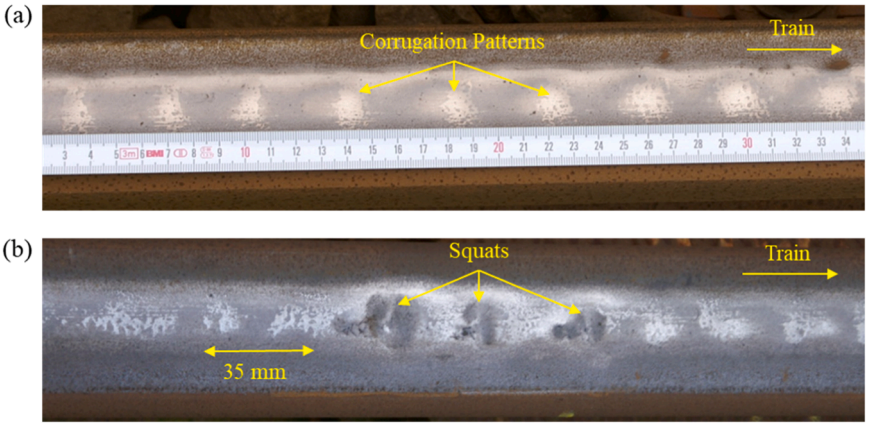

Fig. 1. Rail corrugation and corrugation-induced squats in the Dutch Railway. (a) Rail corrugation with a wavelength of around 40 mm; (b) corrugation-induced squats with crack depths reached about 6 mm based on the ultrasonic test.

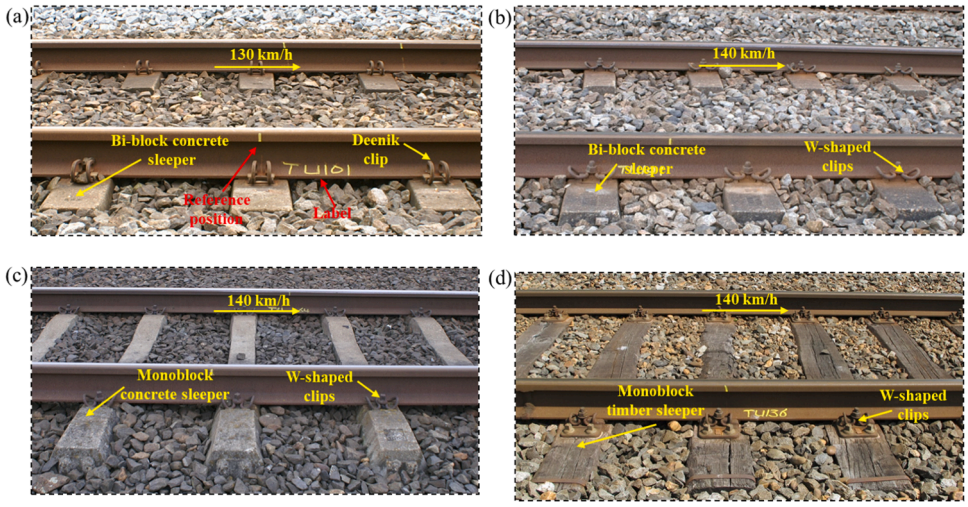

Fig. 2. Four sections of monitored tracks for investigation of rail corrugation. (a) Track 1 at Steenwijk with Deenik fastenings and bi-block concrete sleepers; (b) Track 2 at Assen with W-shaped fastenings and bi-block concrete sleepers; (c) Track 3 at Weert with W-shaped fastenings and monoblock concrete sleepers; (d) Track 4 at Wirdum with W-shaped fastenings and bi-block timber sleepers.

Table 1
The field conditions of the monitored tracks for investigation of rail corrugation.

ID	Locations	Rail	Sleepers	Fastenings	Speed	Annual load
Track 1	Steenwijk after a curve	UIC54E1 R260Mn	Bi-block Concrete	Deenik	130 km/h	3.4 MGT
Track 2	Assen after a curve	UIC54E1 R260Mn	Bi-block Concrete	W-shaped	140 km/h	6.3 MGT
Track 3	Weert before a curve	UIC 54E1 R260Mn	Monoblock Concrete	W-shaped	140 km/h	3.0 MGT
Track 4	Wirdum before a curve	UIC 54E1 R260Mn	Monoblock Wooden	W-shaped	140 km/h	4.2 MGT

2.2. Monitoring method

Between 2007.09 and 2012.11, eleven field observations were conducted at approximately six-month intervals on the four selected tracks, as shown in the timeline in Fig. 3a. The grinding activities were also included in the timeline because of their significant influence on corrugation development. During this monitoring period, two times of grinding were conducted on Track 1 at Steenwijk: the first one happened between the fifth (2009.11) and sixth (2010.06) observations and the second one between the seventh (2010.11) and eighth (2011.06) observations. Track 2 at Assen and Track 4 at Wirdum also underwent two times of grinding, while no grinding activities were performed on Track 3 at Weert during the monitoring period. It was reported in [51] that Track 3 was ground not long before March 2006.

During each observation, corrugations were photographed (about three sleeper spans) to record their development processes. The geometry of the railhead at some selected corrugations was measured using the devices RailProf and MiniProf. RailProf measured the vertical-longitudinal profile along the railhead centre line at 5 mm intervals over a 1 m length. To ensure consistency across different observations, the middle of RailProf was aligned with the yellow marks (see Fig. 2a) during each measurement. In addition, the positions of corrugation-induced squats can serve as references for data alignment for different observations. MiniProf measured the vertical-lateral profile at the yellow marks. By comparing MiniProf measurements with the standard rail profile or across different observations, rail wear and the wheel-rail contact position could be determined.

In addition to photos and rail geometry, the track dynamic behaviours and vehicle-track interaction responses are crucial to fully understanding corrugation development. During the observations, hammer tests were conducted to obtain the FRFs of the monitored tracks at two cross-sections: above the sleeper (on-support) and the midpoint between two sleepers (mid-span), as illustrated in Fig. 3d. The methods for data acquisition and processing are detailed in [52]. At that time, only vertical FRFs were measured, which is insufficient to investigate the influence of the rail longitudinal vibrations on corrugation formation. Therefore, a hammer test was also performed on a section of track with corrugation in Zoetermeer, the Netherlands, in 2023.11, where both vertical and longitudinal FRFs were obtained. More detailed information about this test can be found in 3.4.

ABA measurement is an efficient and cost-effective method for monitoring railway tracks and can provide valuable insights into vehicle-track dynamic interactions, especially in the high-frequency range [31]. Since 2009.03 for Tracks 2 and 3, and 2010.03 for Tracks 1 and 4, ABA measurement (see Fig. 3e) was conducted on the monitored tracks at an interval of about three months. Both vertical and longitudinal ABAs were measured on two driven axles with a distance of 2.56 m. The sampling frequency was 25.6 kHz and the train speed was about 100–110 km/h.

3. Validations of numerical predictions of corrugation development

In [32,33,36], the corrugation formation mechanism was identified based on numerical simulations employing a 3D FE model of vehicle-track dynamic interactions. This model simulates the wheel and rail based on their real geometries and materials using solid elements, applies an automatic surface-to-surface contact scheme, and employs an implicit-explicit sequential approach. It is capable of simultaneously and accurately simulating the wheel-rail frictional rolling contact and

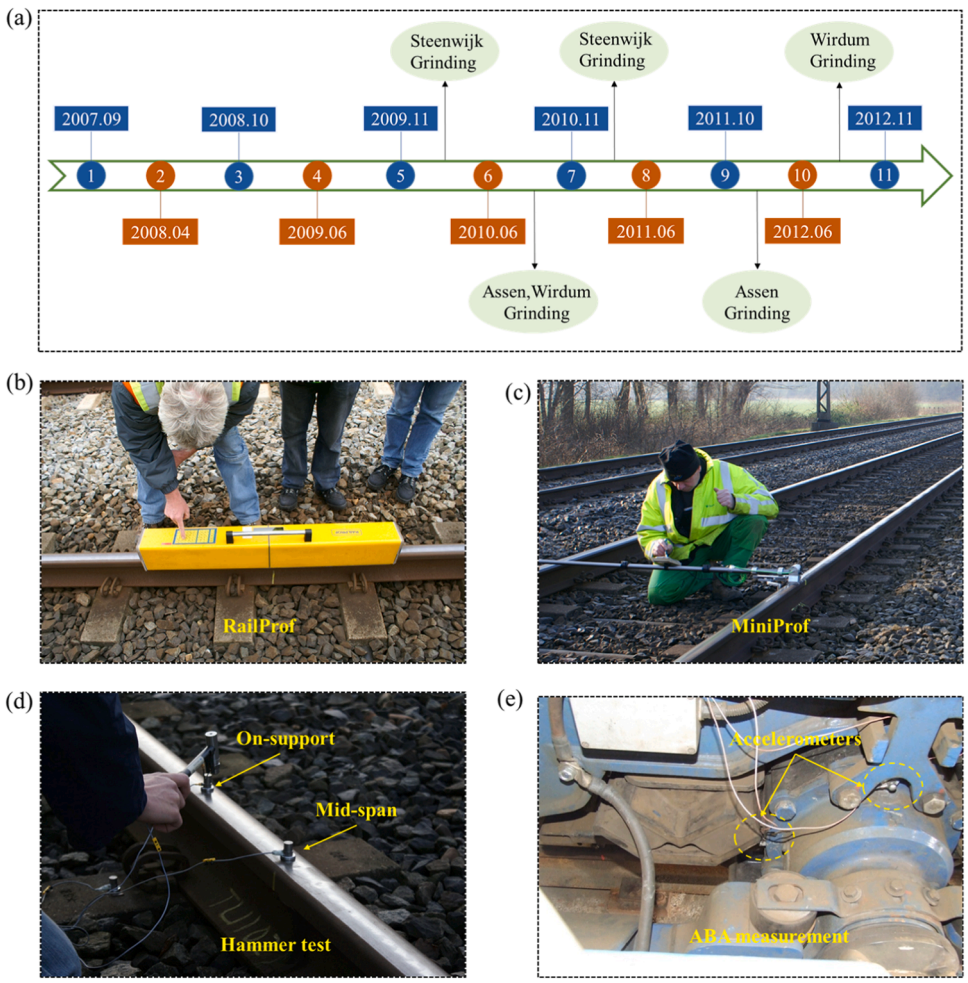

Fig. 3. The monitoring method of the four tracks for investigation of rail corrugation. (a) Monitoring timelines with grinding activities; (b) RailProf; (c) MiniProf; (d) Hammer tests at on-support and mid-span locations; (e) ABA measurement.

high-frequency dynamics of the vehicle-track system. Using this 3D FE model with degraded fastenings, initial corrugation has been successfully reproduced from the smooth rail. The corrugation can consistently grow up to 80 μm, assuming that the damage mechanism is wear. The complete process of corrugation development, including initiation, growth and the limiting amplitude, was explained by the interplay between longitudinal and vertical vibrations. The major findings are summarized as follows.

1. Corrugation will not initiate in nominal track conditions and initial excitation is necessary for corrugation formation.
2. Rail corrugation consistently initiates and grows at fixed locations with the continuous accumulation of differential wear.
3. Wheel-rail longitudinal vibration is dominant for corrugation initiation, and vertical vibration becomes increasingly important with increasing corrugation amplitude.
4. Rail longitudinal vibration modes are decisive to corrugation initiation, and the consistency between the vertical and longitudinal modes determines corrugation growth.
5. Multiple eigenfrequencies can be excited by various initial excitations, causing multiple wavelength components of corrugation at a particular traffic speed.
6. There is a limiting corrugation amplitude, beyond which corrugation barely grows.
7. Artificial corrugation marks will be erased by wheel-rail dynamic interactions and the resulting differential wear.

3.1. Validation of necessary initial excitation for corrugation formation

In [33,36], it was predicted that initial excitation is necessary to excite wheel-rail dynamic forces, cause differential wear on the rail surface, and induce corrugation initiation. Under nominal conditions without initial excitation, corrugation will not initiate. The initial excitation considered in these studies is generally a damaged state of rail fastenings determined by design, construction, and degradation. This may not be the only form of effective initial excitation; other track deterioration conditions that can trigger vehicle-track high-frequency resonances may also lead to corrugation development.

Observations from the four monitored tracks reveal that corrugation is not everywhere on the rail but occurs at particular locations, see some examples in Fig. 4. TU168 (Fig. 4a) and TU169 (Fig. 4c) were both located on Track 2 at Assen, about 40 m apart, and TU021 (Fig. 4b) and TU065 (Fig. 4d) were on Track 4 at Weert, around 400 m apart. Corrugations were observed and measured at TU168 and TU021, but not at TU169 and TU065. Besides, it was worth noting that the rails on Track 1 at Steenwijk, laid in place in 1987, were not ground until November 2009. Similar observations in the Dutch railway were reported in [18,53], showing that rail corrugation was not found everywhere after about 20 years of service without grinding. These observations are consistent with the numerical simulation, suggesting that initial excitation is necessary for corrugation formation. The hypothesis in the literature, proposing that the initial stochastic rail surface roughness alone excites the so-called corrugation 'wavelength-fixing' mechanism [18,54], seems insufficient to explain corrugation, as the monitored rails on the same

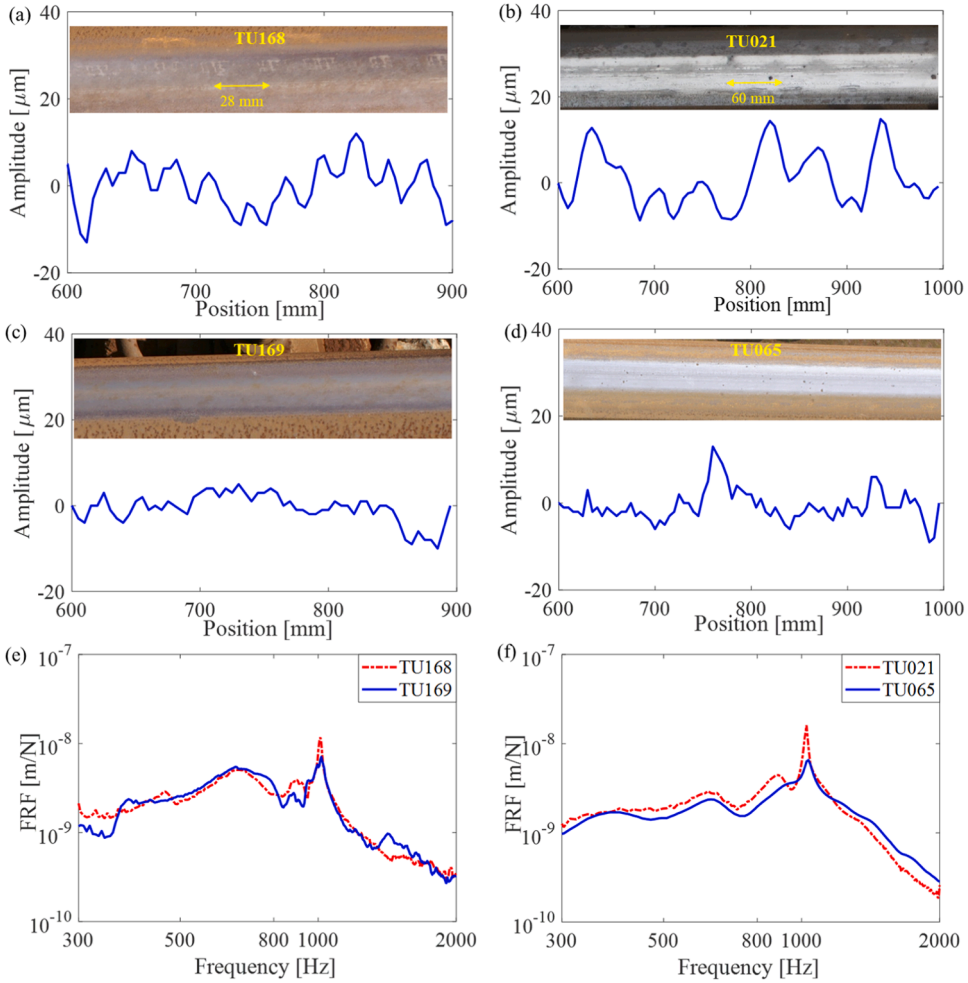

Fig. 4. Field observations of tracks with and without corrugations. (a) TU168 with corrugation on Track 2 at Assen; (b) TU021 with corrugation on Track 4 at Weert; (c) TU169 without corrugation on Track 2 at Assen; (d) TU065 without corrugation on Track 4 at Weert; (e) the vertical FRFs at TU168 and TU169; (f) the vertical FRFs at TU021 and TU065.

track had approximately identical initial roughness from the manufacturing process.

The initial excitation that induces corrugation will change the track dynamic behaviours from the nominal states [34], which could thus be identified from the track FRFs measured by hammer tests. Figs. 4e and 4f compare the vertical FRFs of the tracks with and without corrugation during the first observation. It can be seen that the peaks in FRFs of corrugated tracks are sharper than those of non-corrugated tracks, despite similar peak frequencies. These peaks correspond to different track resonance modes [42], with their frequencies and sharpness primarily determined by vertical stiffness and damping of fastenings [55], respectively. The results in Figs. 4e and 4f indicate that the fastenings of the corrugated tracks were degraded by providing less damping, making track resonance modes more predominant. This agrees with the numerical simulations [33] that fastening degradations serve as necessary initial excitation for corrugation formation. Besides, corrugation formation seems not determined by fastening vertical stiffness, which is similar for both corrugated and non-corrugated tracks. Comparison of longitudinal FRFs for tracks with and without corrugation reveals that initial excitation releases the rail longitudinal vibration mode, which is decisive to corrugation formation. A more detailed analysis of this comparison is provided in 3.4. Overall, the field observations validate the numerical simulations, indicating that initial excitation is necessary for corrugation formation. Although numerical simulations in [36] and laboratory experiments in [35,37] offer preliminary insights into the quantitative relationship between fastening degradation and rail corrugation, further field investigations on track longitudinal dynamics could be performed in future work to more precisely quantify the relationship between the degree of fastening degradation/initial excitation with corrugation initiation.

3.2. Validation of corrugation consistent growth with differential wear

In [33], it was predicted rail corrugation consistently grows at fixed locations with the continuous accumulation of differential wear. This subsection provides field data on corrugation growth to validate the prediction.

3.2.1. Consistent growth at fixed locations

Fig. 5 depicts the corrugation growth process at four sites from the four monitored track sections. Figs. 5a, 5b and 5c show that corrugations at TU101, TU193 and TU064 consistently grew: the corrugation peaks and troughs did not move over time, steadily growing at fixed locations. The consistency even held for some minor peaks, for instance, the one at around 130 mm in Fig. 5c. This consistent growth trend is also observed for the corrugation at TU137, although it is less clear due to the less distinguishable wave patterns of initial corrugation in 2007.09.

Moreover, different growing tendencies are observed in these four corrugations. The corrugation amplitude (i.e., peak-to-trough distance) at TU101 increased little for over two years, with a maximum of 7 μm at around 180 mm. In contrast, corrugation amplitudes at TU193, TU064 and TU137 considerably increased by about 25 μm, 35 μm and 18 μm,

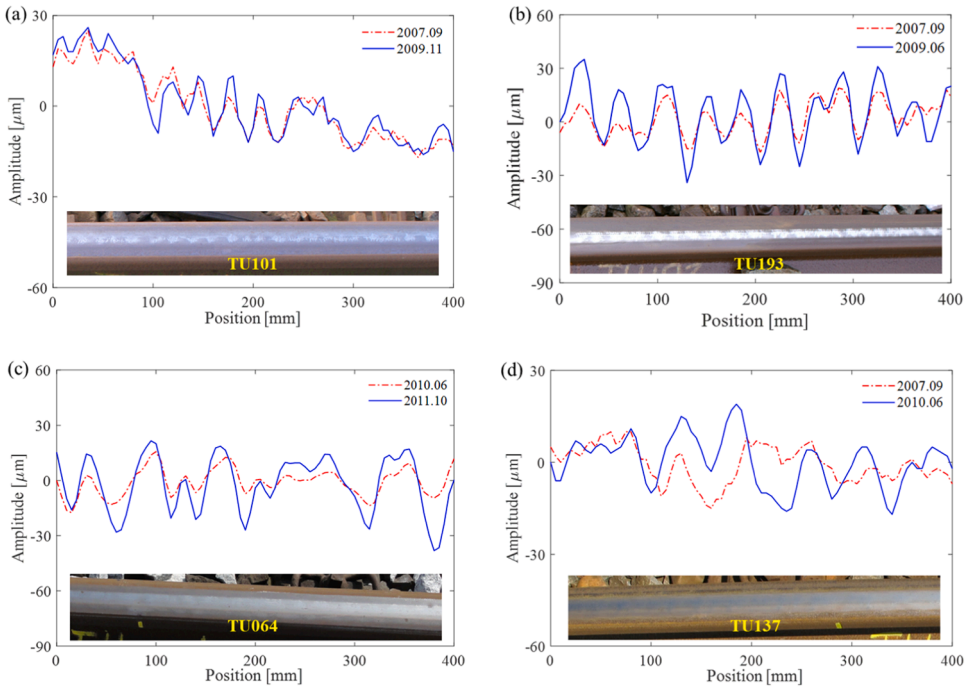

Fig. 5. Field validation on corrugation consistent growth at fixed locations. (a) TU101 on Track 1 at Steenwijk; (b) TU193 on Track 2 at Assen; (c) TU064 on Track 3 at Weert; (d) TU137 on Track 4 at Wirdum.

respectively. The reason could be that the corrugation at TU101 almost reached its limiting amplitude and thus barely grew, whereas the corrugations at the other three sites were still in the rapid growth stage. An analysis of corrugation limiting amplitude is presented in 3.6.

3.2.2. *Validation of the differential wear*

Fig. 6 shows the vertical-lateral rail profiles measured by MiniProf at the same four corrugation sites as in Fig. 5. Rail wear is calculated by comparing these profiles across different observations or against the standard UIC54E1 profile. At TU101 (Fig. 6a), the rail wear before 2007.09 was about 0.99 mm. From 2007.09–2009.11, the wear increased by about 0.15 mm, averaging 0.07 mm/year, representing the natural wear rate without grinding. At TU193 (Fig. 6b), the rail wear before 2007.09 was approximately 4.00 mm. Between 2007.09 and 2009.06, the natural rail wear was about 0.26 mm, averaging 0.15 mm/year. For TU064 (Fig. 6c) and TU137 (Fig. 6d), the rail wear before 2008.10 was about 0.72 mm and 0.38 mm, respectively. From 2008,10 to 2010.06, the wear increased by 0.14 mm at TU064 and 0.18 mm at TU137, corresponding to wear rates of 0.08 mm/year and 0.11 mm/year, respectively.

Fig. 6e shows the rail wear rates at these four sites by considering the annual traffic load, which ranges from around 2.06–2.67 mm/100MGT. For comparison, the statistical data from the Belgian railway network are also presented in this figure, indicated by two red dashed lines. In Belgium, the vertical wear on straight tracks for the R260 rail under the UIC5 load was from 0.96 to 2.18 mm/100MGT, with an average of 1.57 mm/100MGT [56]. It can be seen that the rail wear rates in the Dutch and Belgian railways are generally comparable. The wear rate in the Dutch railway was slightly higher because the monitored straight tracks were located close to curves, where the friction force was expected to be higher than typical straight tracks due to train traction and braking.

Compared with Fig. 5, it is evident that the rail wear rate (e.g., 150 μm/year at TU193) is considerably larger than the corrugation growth rate (e.g., 14 μm/year at TU193). Fig. 6f depicts a schematic drawing of corrugation consistent growth due to the differential wear. The two grey dashed lines illustrate the average rail wear. It can be seen that the corrugation trough is worn more than the peaks, and the additional wear at the trough compared to the peak corresponds to the increasing corrugation amplitude. For instance, at TU193, the corrugation trough was worn 14 μm more than the peak annually, about 9.3 % faster, considering an annual rail wear of 150 μm.

It is worth noting that all four monitored tracks in this study were made of R260Mn steel, which should have a nearly identical wear rate under the same traffic load. Previous studies have reported that corrugation formation is sensitive to rail materials. Given that corrugation develops through differential wear, it can be inferred that softer rail materials with higher wear rates are more susceptible to corrugation formation. This is consistent with the laboratory experiments in [37], which showed that corrugation occurred only on the softest steel material R220. To further investigate the influence of rail material on corrugation formation, more field observations and analyses could be conducted in future studies.

3.3. *Validation of the roles of longitudinal and vertical vibrations in corrugation formation*

It was predicted in [33] that vehicle-track longitudinal vibration is dominant for corrugation initiation, while vertical vibration becomes increasingly significant as the corrugation grows. To validate this prediction, the corrugation at TU193 on Track 2 is analyzed with different amplitudes, including both the initiation and growth stages, as shown in Fig. 7.

In 2009.06, severe corrugation was observed, with a peak-to-trough distance up to 51 μm (Fig. 7a). Four major wavelength components were identified: 53 mm, 43 mm, 34–37 mm, and 28 mm (Fig. 7b). The rail was ground within one month after the 6th (2010.06) observation, as shown in Fig. 3a. Afterwards, corrugation reoccurred at the same location (indicated with the black dashed lines in Fig. 7a) and grew, as evidenced by the measured corrugation geometry in 2010.11 and 2011.10. It is noted from Fig. 7b that corrugation had nearly identical wavelength components before (2009.06) and after (2011.10) grinding, as indicated by the black dashed lines in Fig. 7b. The difference in corrugation geometry in Figs. 7a and 7b before and after grinding is

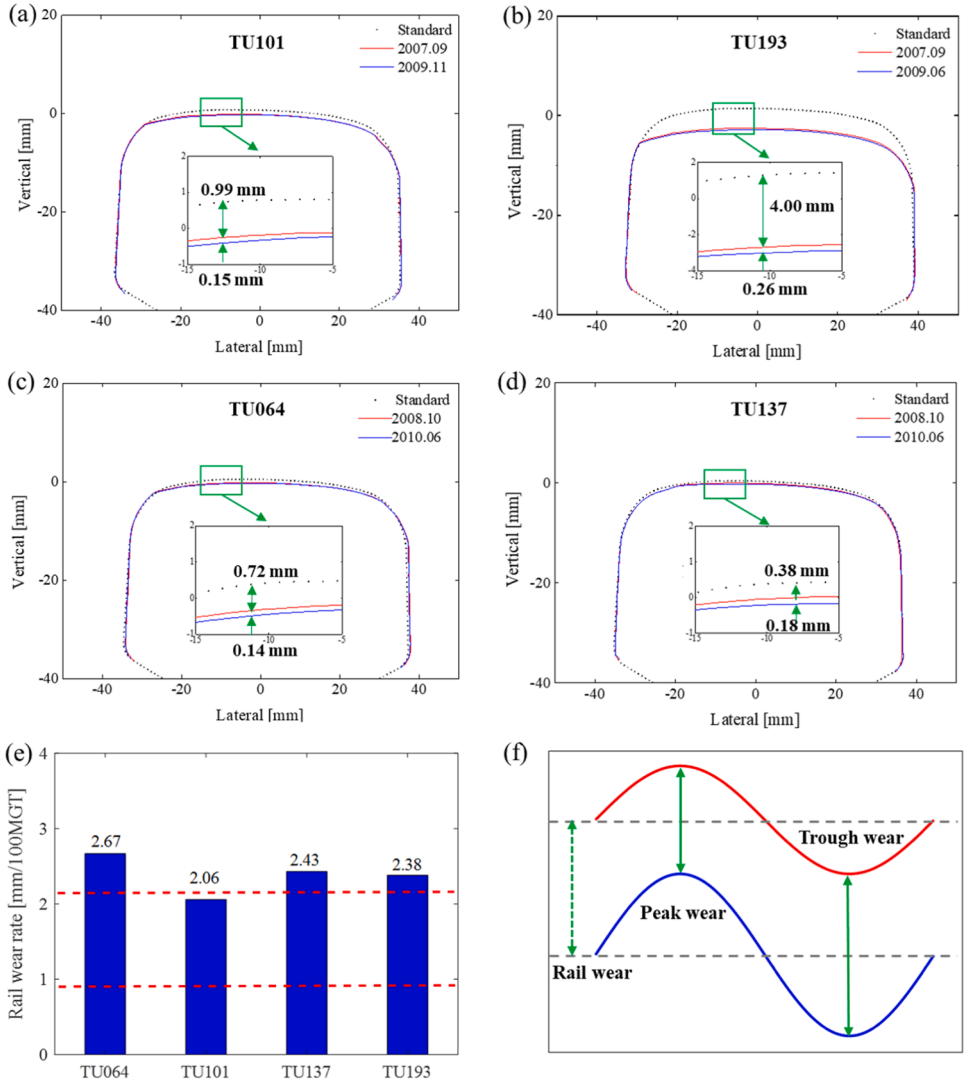

Fig. 6. The vertical-lateral rail profiles measured by MiniProf and the calculated rail wear. (a) TU101 on Track 1 at Steenwijk; (b) Assen TU193 on Track 2 at Assen; (c) TU064 on Track 3 at Weert; (d) TU137 on Track 4 at Wirdum; (e) the rail wear rates at these four corrugation sites, and the two red dashed lines indicate the statistical data from the Belgian railway network; (f) schematic drawing of corrugation consistent growth due to differential wear.

caused by the grinding, and it became smaller with time. This trend is particularly clear in Fig. 7b: the power spectral density (PSD) of 2010.11 has almost no correlation with that of 2009.06, whereas the PSD of 2011.10 shows a strong correlation with that of 2009.06 with the (almost) identical wavelengths of the corrugation components around 28 mm, 34–37 mm, 43 mm and 53 mm. The small wavelength difference between the PSD of 2009.06 and 2011.10 should be due to (1) they were in different stages of the corrugation development; and (2) the splitting of the corrugation wavelength at 34 mm into two: 34 mm and 37 mm. Such wavelength/frequency splitting can happen when corrugation is severe so that the intensity of the dynamic interaction increases [33].

Eight rounds of ABA measurements are analyzed, and their PSDs are shown in Figs. 7c-7f and Fig. 8. Figs. 7c and 7d show the PSD of the vertical and longitudinal ABAs at TU193 measured in 2009.08, 2010.10 and 2011.11. These three ABA measurements were chosen because they were the closest in time to the three observations in Figs. 7a and 7b. Each PSD was calculated as the average of six ABA signals (from accelerometers on two axles in three measurement runs) to minimize random errors. It shows that the overall vibration amplitude of ABA was the largest in 2009.08 with the severest corrugation, significantly decreased to a minimal level in 2010.10 due to rail grinding, and then increased again in 2011.11 because of the reoccurrence of corrugation.

In 2009.08, the severe corrugation excited vertical and longitudinal ABAs around the four corrugation wavelengths. The vertical ABA magnitude was notably the highest near 53 mm and relatively smaller near 28 mm. In contrast, the longitudinal ABA exhibited the highest energy at 28 mm and the lowest at 53 mm. This result suggests that longitudinal ABA is more responsive to the shorter-wave components of corrugations compared to vertical ABA, consistent with the finding in [31] that longitudinal ABA is more sensitive in detecting light squats with shorter wavelengths of about 10–30 mm. In 2010.10, which was only a few months after the rail grinding, both the longitudinal and vertical ABAs were significantly low because the re-occurring corrugation was still in its early stages. In 2011.11, the corrugation had significantly developed, especially at the 53 mm wavelength, as depicted in Figs. 7a and 7b, and excited the ABAs with larger amplitudes. Again, the longitudinal ABA was much more sensitive to the 28 mm wavelength. The vibration energy of the ABA signals was relatively weak at the 34 mm wavelength. A possible reason could be that the ABA measurement speed of 100–110 km/h was different from the normal traffic speed of 140 km/h, which thus influenced some of the wheel-rail resonance amplitudes [36]. Figs. 7e and 7f show the PSDs of the ABA in 2010.06 when the grinding roughness dominated, and in 2010.10 when

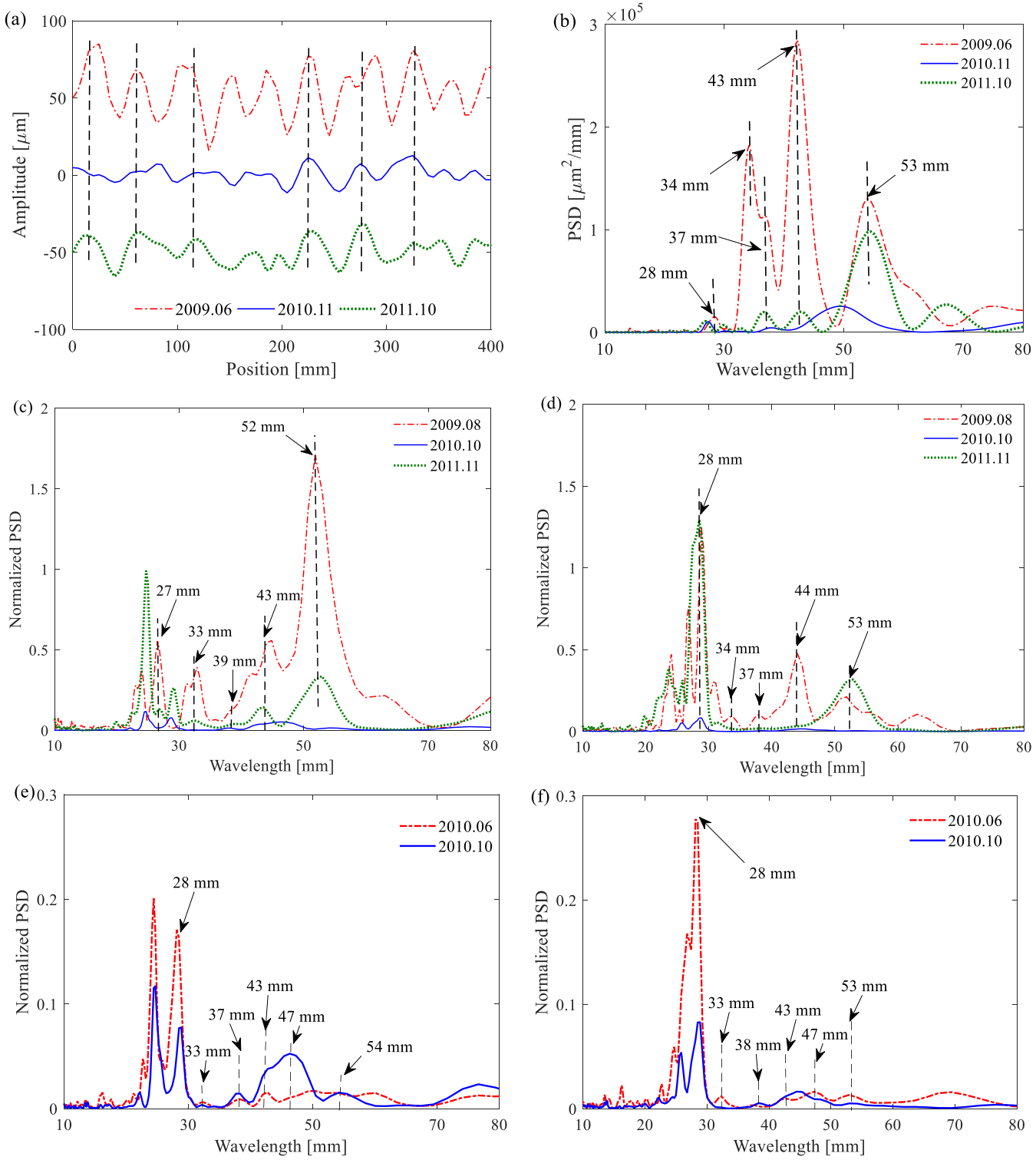

Fig. 7. The evolution of corrugation geometry and ABAs before and after grinding at TU193 on Track2 in Assen. (a) corrugation geometry in the spatial domain; (b) corrugation geometry in the wavelength domain; (c) vertical ABA in the wavelength domain in 2009.08, 2010.10, and 2011.11; (d) longitudinal ABA in the wavelength domain in 2009.08, 2010.10, and 2011.11; (f) vertical ABA in the wavelength domain in 2010.06 and 2010.10; (g) longitudinal ABA in the wavelength domain in 2010.06 and 2010.10.

grinding marks had largely been worn away. The wavelengths seen in Figs. 7b, 7c and 7d are all present in Figs. 7e and 7f. The extra 47 mm wavelength in 2010.10 disappeared later; therefore it could be due to a temporary defect on the rail, instead of being from a vibration mode.

Fig. 8 shows the average PSDs of the longitudinal and vertical ABAs for five wavelength ranges: the overall 10–80 mm range (Figs. 8a), and 4 sub-ranges 51.5–54.5 mm (Figs. 8b), 42.5–45.5 mm (Figs. 8c), 30.5–38 mm (Fig. 8d) and 20–31 mm (Fig. 8e), respectively. The first range reflects the overall vibration levels in 10–80 mm, and the other four ranges correspond to the characteristic corrugation wavelengths. It is observed from Fig. 8a that the average PSDs of ABAs in 10–80 mm grew with time in 2009.08, 2009.10, and 2010.03, then dropped to

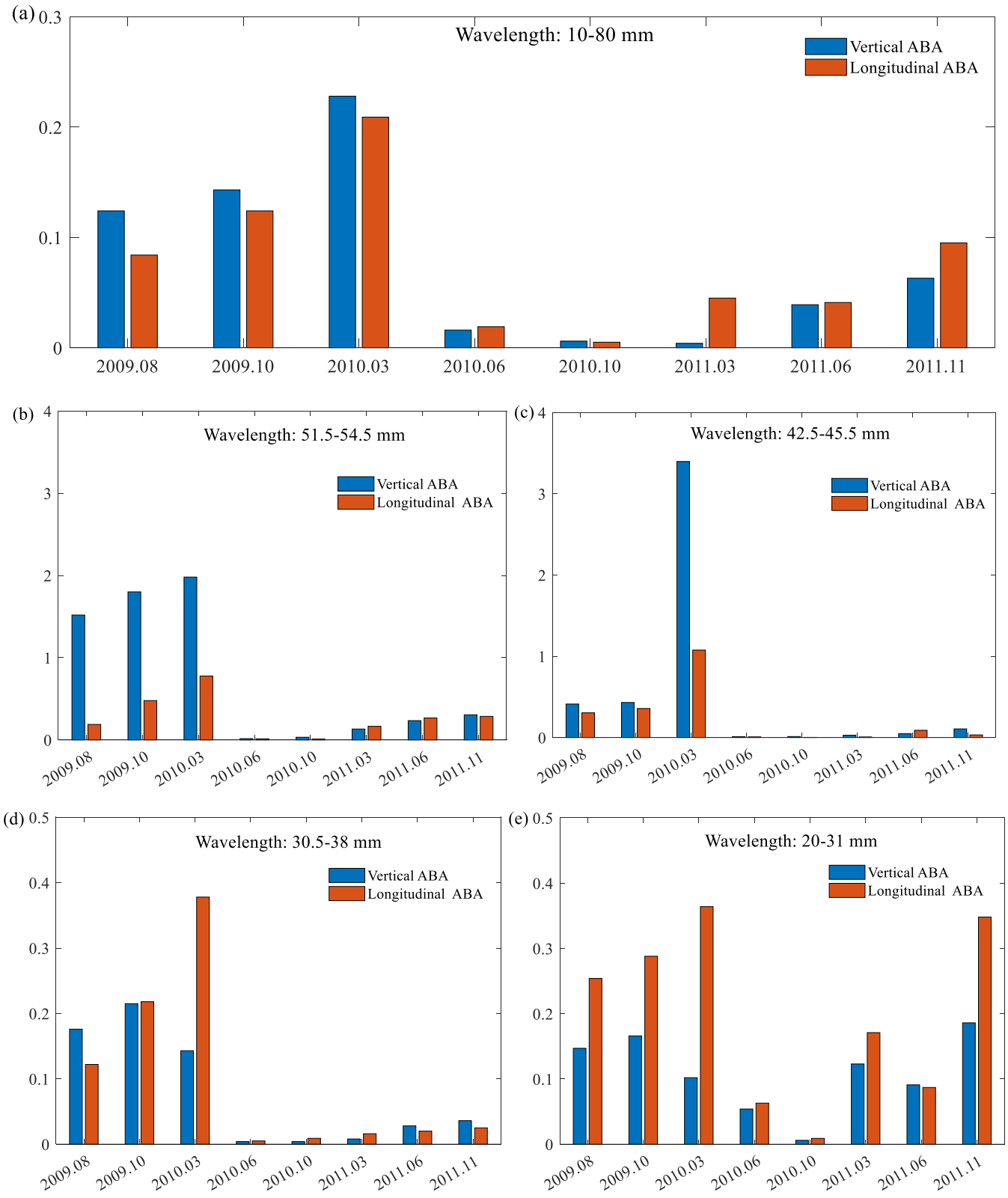

Fig. 8. The average PSDs of ABAs before and after grinding at TU193 within different wavelength ranges. (a) Average PSDs in 10–80 mm; (b) average PSDs in 51.5–54.5 mm; (c) average PSDs in 42.5–45.5 mm; (d) average PSDs in 30.5–38 mm; (e) average PSDs in 20–31 mm.

almost zero due to grinding. The lowest PSDs are not those immediately after the grinding in 2010.06, but four months later in 2010.10. The relatively higher PSDs in 2010.06 were due to the roughness caused by the grinding, which will be further discussed in 3.7. In 2010.10, the grinding roughness was worn away, while corrugation did not yet initiate. Five months later, in 2011.03, corrugation reoccurred and continued to grow in 2011.06 and 2011.11.

Moreover, it is found in the wavelength range 10 – 80 mm (Fig. 8a)

that the vertical ABA PSD exceeded the longitudinal ABA PSD before grinding when the corrugation was severe, while this trend reversed after the grinding and when corrugation was re-initiating. This result suggests that longitudinal vibration plays a crucial role in corrugation initiation, whereas vertical vibration becomes increasingly important during corrugation growth. The early detection or prediction of corrugation is thus possible based on vehicle-track longitudinal dynamic response, e.g., longitudinal ABA. A pattern similar to Fig. 8a is found for the longer wavelengths of 51.5–54.5 mm and 42.5–45.5 mm, as shown in Figs. 8b and 8c.

However, for the shorter wavelengths, as shown in Figs. 8d and 8e, longitudinal ABA could exceed vertical ABA even at larger corrugation amplitudes, e.g., before grinding when the corrugation was the severest. This could be because of the greater sensitivity of ABA to short-wave defects [31] or partly due to the possibility that the longitudinal rail vibration was inherently stronger at shorter wavelengths. It can be seen from Figs. 8b-8e that with decreasing wavelength, the PSD changes overall from vertically dominant to longitudinally dominant, irrespective of the corrugation severity and grinding effect. This result seems to confirm the possibility that longitudinal vibration for shorter wavelengths is inherently strong in comparison to vertical vibration. This can then explain why the corrugations are of short pitch: the longitudinal vibrations of short wavelengths are stronger in comparison to vertical vibration, not only when without corrugation and with slight corrugation, but also when the corrugation is severe so that the longitudinal vibration-induced differential wear accumulates dominantly and consistently even when the corrugation becomes severe. If the vertical vibration-induced differential wear becomes dominant during the corrugation development, the corrugation growth will be disturbed and disrupted because the vertical vibration wavelengths can be different from those of the longitudinal ones – the wear induced by the vertical vibrations is inconsistent with the initial wear that is induced by the longitudinal ones [33]. This short pitch sets the upper bound of the corrugation wavelength by the relative strength of the vertical vibrations versus the longitudinal vibrations. The contact filter effect probably sets the lower bound [25].

In light of the above discussion, Let's assume that the corrugation developed from (almost) no corrugation in 2010.11 (ABA of 2010.10), to moderate corrugation in 2011.10 (ABA of 2011.11), till severe corrugation in 2009.06 (ABA of 2009.08), i.e., considering the corrugation of 2009.06 as a further growth of that of 2011.11. We check whether such a development sequence follows the corrugation mechanism presented in [33] and find that:

1. Effects of grinding generally disappeared after 4 – 5 months.
2. Between 24 ~ 30 mm there are multiple vertical and longitudinal wavelength components. Because they are close to each other, their resonance interferes with each other, causing the canceling effect of their differential wear so that the corrugation components in this wavelength range can hardly grow (see Fig. 7b).
3. Despite the small corrugation magnitude around 28 mm wavelength, it excites strong ABA, especially longitudinal ABA (see Figs. 7c, d and 8e). Therefore ABA can be a good measure of early short-wave defects, confirming the finding of [31].
4. There are 2 closely-spaced wavelengths: 34 mm and 37 mm in Fig. 7b. The 37 mm wavelength corresponds to a longitudinal mode, as indicated in Fig. 7d, which drove the initial growth of the 37 mm component. This component was very weak in Fig. 7b in 2010.11 and became clearly visible in 2011.10. "Later" in 2009.06, when the corrugation became severe, the vertical excitation became strong, and both vertical and longitudinal vibrations were induced around 34 mm wavelength so that differential wear of 34 mm grew quickly to be stronger than the 37 mm component; see the 33 mm and 34 mm wavelengths in Figs. 7c and 7d. This development of the 34 mm component due to strong dynamics in association with a nearby eigenmode (37 mm) is called wavelength (or frequency) splitting [33].
5. The 43 mm and 53 mm components were absent in the 2010.11 PSD of the corrugation (see Fig. 7b) because it did not initiate yet, but it was in both the vertical and longitudinal ABA (see Fig. 7c ~7 f). This indicates that there are both vertical and longitudinal eigenmodes around wavelengths of 43 mm and 53 mm. Resonances at these eigenmodes resulted in the development of the corrugation components in 2011.10 and then 2009.06. The very large PSD of the 2009.6 corrugation at 43 mm induced only a moderate vertical resonance peak in the ABA PSD (see Fig. 7c), indicating that the wavelength of the vertical eigenmode may not match very well the 43 mm wavelength of the corrugation. This means that the longitudinal eigenmode between 43 and 45 mm could have induced this corrugation. In contrast, the moderate PSD of the 2009.6 corrugation at 53 mm induced strong vertical resonance mode, leading to a very high PSD peak of the vertical ABA.

Overall, the findings above agree with the proposed mechanism of [33]. The corrugation, after grinding, re-initiated and grew in a way that is consistent with the corrugation before the grinding, as if the 2009.06 corrugation was developed from the 2011.10 corrugation. The grinding was a disruption and disturbance to the corrugation development. The effect of the grinding roughness, however, was only temporary and disappeared after 4 – 5 months. The corrugation wavelengths were determined by the eigenmodes of the vehicle-track system and speed [33], not grinding.

3.4. Validation of the dominance of rail longitudinal mode on corrugation formation

It was predicted in [33] that rail longitudinal vibration modes are dominant for corrugation initiation, and the consistency between the vertical and longitudinal modes determines corrugation growth. As introduced in 2.2, only vertical FRFs were measured on the four monitored tracks. To validate this prediction, we performed hammer tests on another track with corrugation in November 2023 (Fig. 9), where both the vertical and longitudinal FRFs were obtained.

This track is a section of straight track located in Zoetermeer, the Netherlands. It consists of UIC54 rail, W-shaped fastenings and monoblock concrete sleepers. The track is about 2 km before the Zoetermeer station, and the traffic speed is about 105 km/h. It is observed in Fig. 9a that the corrugation wavelength is approximately 30 mm. The corrugation characteristic frequency is about 1000 Hz, calculated by dividing the traffic speed v with the corrugation wavelength λ, as follows.

$$f = \frac{v}{\lambda} \tag{1}$$

Figs. 9b and 9c show that both the longitudinal and vertical FRFs have a predominant resonance peak at around 1000 Hz, supporting the numerical prediction that the consistency between the vertical and longitudinal modes determines corrugation growth. Moreover, when comparing with FRFs of tracks without corrugation, the vertical resonance peak at 1000 Hz, corresponding to the vertical pinned–pinned resonance mode, occurs at both corrugated and non-corrugated tracks. However, the longitudinal mode at 1000 Hz only appears in the track with corrugation. This indicates that the longitudinal vibration mode is decisive in the corrugation formation. Corrugation can thus be mitigated or even eliminated Corrugation can thus be mitigated or even eliminated by designing new frail constraints with high longitudinal stiffness [34]. In future research, more field validation on the dominant role of rail longitudinal modes can be conducted at other corrugation sites.

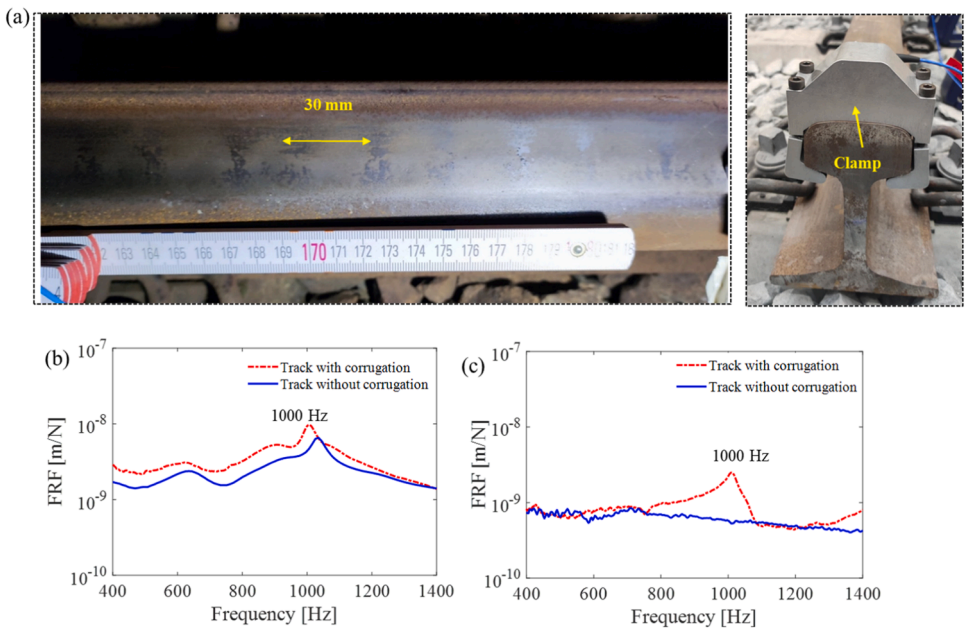

Fig. 9. Validation of the dominance of rail longitudinal mode on corrugation formation. (a) Corrugation on the track near Zoetermeer station, the Netherlands, and a clamp was made for the rail longitudinal excitation; (b) vertical FRFs of tracks with and without corrugation; (c) longitudinal FRFs of tracks with and without corrugation.

3.5. Validation of multiple wavelength components of corrugation at a particular traffic speed

It was predicted in [32,33] that multiple eigenfrequencies of rail longitudinal modes can be excited by initial excitations with various fastening degradation modes, causing multiple wavelength components of corrugation at a specific traffic speed. In contrast, many models in the literature often predicted single wavelength component of corrugation, for instance, those caused by pinned-pinned resonance [17,18].

To validate this prediction, statistical data on corrugation wavelength components were collected from the four monitored tracks, as shown in Fig. 10. It can be seen that the corrugation wavelengths indeed have multiple components ranging from 20 to 80 mm at speeds of about 130–140 km/h. The majority (over 64 %) of the corrugation wavelengths in all the four tracks fall within the 30–60 mm range. Moreover, it is noted that in Track 1 and Track 2, about 70 % of the corrugation wavelengths are within a shorter range of 20–50 mm, whereas in Track 3 and 4, about 70 % are within a longer range of 40–70 mm. The main

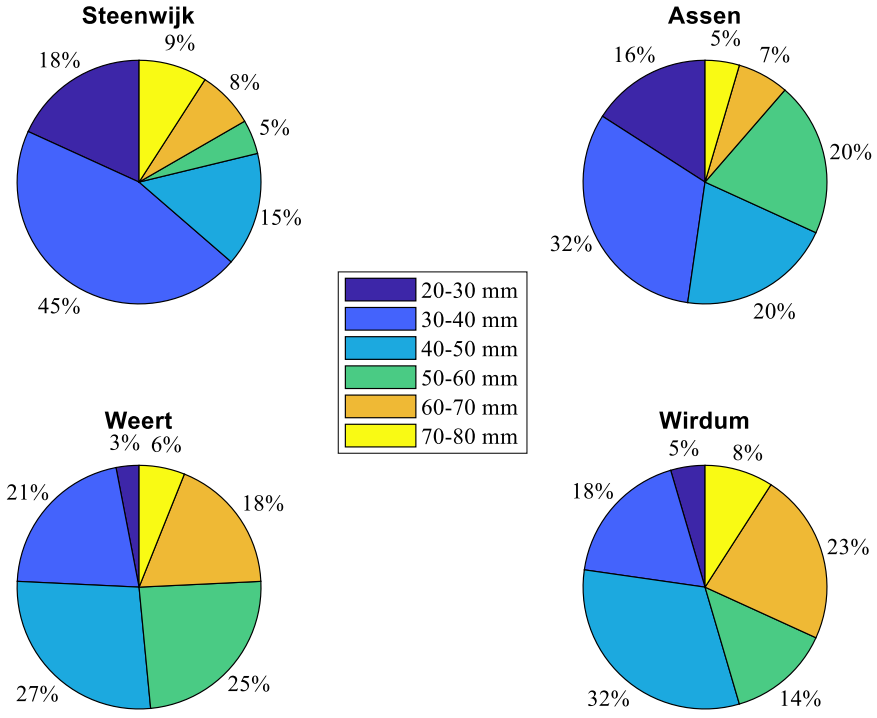

Fig. 10. The statistical data of corrugation wavelength components in the four monitored tracks. Track 1 was at Steenwijk, Track 2 at Assen, Track 3 at Weert, and Track 4 at Wirdum.

difference between them is the sleeper types used: Track 1 and 2 used bi-block sleepers while Track 3 and 4 used monoblock sleepers. The possible reason is that monoblock sleepers provide greater flexibility to the track than bi-block ones due to bending, resulting in lower eigen-frequencies of the tracks and thus longer wavelengths. Furthermore, a comparison between Track 1 and Track 2 reveals that Track 1 has more corrugation wavelengths in the 30–40 mm range and fewer in the 50–60 mm range. This difference is likely caused by different fastening types, which can influence corrugation characteristics [36]. Besides, the effective track length engaged in the dynamic vehicle–track interaction, which could be influenced by, e.g., rail joints or defective welds, may also affect the corrugation wavelength feature. It is observed that Track 3 has wavelength components similar to those of Track 4, possibly suggesting that corrugation is insensitive to sleeper materials, as also reported in [57].

Overall, the field data validate the numerical predictions of multiple wavelength components at a mainline traffic speed. Field observations also indicate that corrugation wavelengths are closely related to the types of fastenings and sleepers, since they influence high-frequency vibrations of vehicle-track system. Future research should carefully consider these components in new track designs for corrugation mitigation.

3.6. Validation of the existence of the corrugation limiting amplitude

It was predicted in [33] that there is a limiting amplitude for corrugation, beyond which corrugation will not further grow. To validate this prediction, the growth of corrugations on Track 1 at Steenwijk was analyzed. Track 1 is so chosen that it had not been ground for over 20 years, and corrugation might reach a limiting amplitude if such an amplitude exists.

Fig. 5a in 3.2.1 shows that the corrugation at TU101 grew little in about two years, with a maximum peak-to-trough distance of 22 μm. Fig. 11 presents two more corrugations at TU104 and TU112 on Track 1, which barely grew in 1.5 years, with maximum amplitudes of about 25 μm and 23 μm, respectively. These results validate the existence of a limiting amplitude for corrugation, which is around 22–25 μm on Track 1. The corrugations at TU193 (Fig. 5b) and TU064 (Fig. 5c) kept growing until grinding, making it impossible to determine their limiting amplitudes, which should exceed 51 μm and 49 μm, respectively. It is predicted in [36] that corrugation limiting amplitude depends on the intensity of the initial excitation, track degradation during the period of the corrugation, and the consistency between the longitudinal and vertical modes.

3.7. Validation of the removal of artificial corrugation marks

In practice, grinding activities may leave some marks on the rail with wavelengths falling in the short pitch range. It is predicted in [32] that such artificial corrugation marks of the rail surface will be erased by the wheel-rail dynamic interaction and the resulting differential wear. Besides, Fig. 8 in 3.3 shows that grinding marks disappeared due to natural wheel-rail wear, and this subsection analyzes the evolution of these artificial grinding marks to examine this numerical prediction.

Fig. 12 shows the remaining grinding marks at TU102, TU108, TU188, and TU 138 on the monitored Tracks 1, 2 and 4. No grinding activities were conducted on Track 3 at Weert during the monitoring period. TU102 and TU108 were both on Track 1 at Steenwijk, but at different times, as shown in the timeline of Fig. 3a. It is observed from Fig. 12 that the wavelengths and amplitudes were different for these grinding marks, and longer wavelengths correspond to larger amplitudes. The wavelength of grinding marks is mainly determined by the grinding train speed [58]. The longer wavelengths correspond to higher grinding speeds and more traction power, likely leading to deeper grinding marks on the rail. Additionally, compared to the 'natural' corrugation shown in Fig. 5, these artificial marks are much more uniform in wavelengths and amplitudes. Figs. 12a, 12b and 12d also presents the evolution of grinding marks at TU102, TU108 and TU138 in about half year. It is evident that the amplitude of artificial marks reduced, indicating they had been worn off by wheel-rail dynamic interaction, consistent with the numerical predictions in [32].

4. Other field observations of rail corrugation

In this section, more field observations about corrugation features are presented, including the presence of corrugation on the left and right rails, and corrugation-induced squats. These observations present additional field evidence to enhance our understanding of rail corrugation, and could serve as a reference for evaluating various corrugation hypotheses.

4.1. Corrugation on the left and right rails

Based on field observations in the four monitored tracks, there seems no direct correlation between the corrugation formation on the left and right rails of straight tracks. At some locations, rail corrugation occurs on one side (see Fig. 13a), whereas at other locations corrugation occurs on both rails (see Fig. 13b). Besides, corrugation on both rails often exhibit different features in terms of the wavelengths and severity, as shown in Fig. 13c and Fig. 13d. The possible reason is explained in [36] that the left and right tracks could have different dynamic behaviours because of various degradation modes, resulting in different characteristics of wheel-rail dynamic interactions, wear and corrugation.

4.2. Corrugation-induced squats

Corrugation excites large wheel-rail dynamic force, causing plastic deformation and work hardening of rail materials under repeated loading cycles. This process gradually deteriorates the RCF resistance of the rail, increases its brittleness, and finally induces black depressions and squats. A more detailed explanation of the formation mechanism of corrugation-induced squats can be found in [9]. This subsection

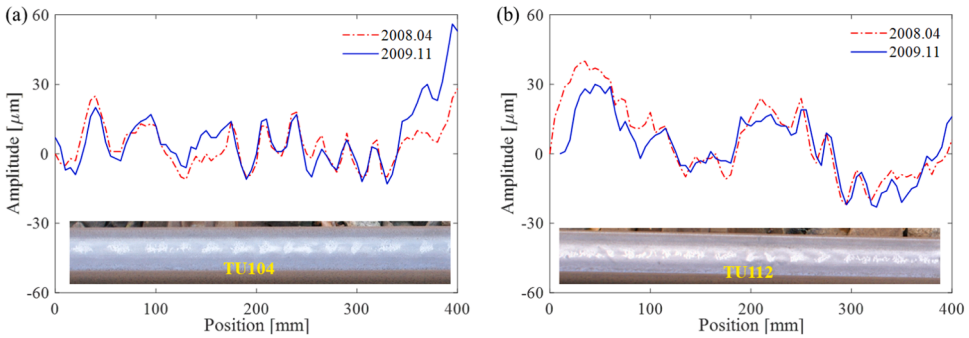

Fig. 11. Validation of the existence of the corrugation limiting amplitude. (a) TU104 on Track 1 at Steenwijk; (b) TU112 on Track 1 at Steenwijk.

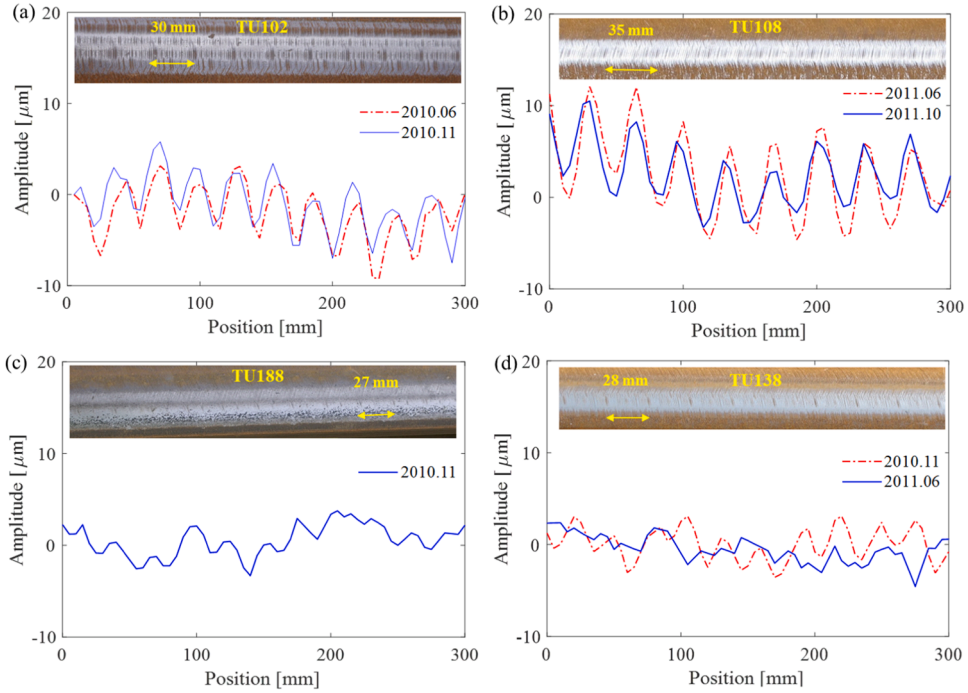

Fig. 12. Grinding marks on the rail surface. (a) TU102 on Track 1 at Steenwijk; (b) TU108 on Track 1 at Steenwijk; (c) TU188 on Track 2 at Assen; (d) TU138 on Track 4 at Wirdum.

provides more insights into the evolution of corrugation geometry with the development of squats.

Field observations indicate that squats typically form at corrugation peaks, see the example in Fig. 14a. Three small black depressions first initiated at corrugation peaks, and gradually developed into kidney-like mature squats. The preference for squats to develop at corrugation peaks is due to the larger dynamic contact stress at corrugation peaks [59], causing faster plastic deformation and work hardening. The grey dashed lines in Fig. 14b illustrate the original positions and shapes of corrugation peaks. Corrugation peaks had become depressions in the first observation (September 2007) with depths comparable to the corrugation amplitude, and it seems that the overall corrugation wavelength became shorter. From the first to fifth (November 2009) observations, squats gradually grew in both the traffic and anti-traffic directions and became increasingly wide and deep. During this process, the original corrugation peaks following the squats were worn off by wear and plastic deformation, and the troughs were merged into the adjacent squats. By the fifth observation, the corrugation patterns were no longer distinguishable in the rail geometry measurements, although still visible in the photos in Fig. 14a. After the fifth observation, the rail was ground about 1.1 mm, and the squats remained clearly visible in the six observation and measurable from the rail geometry, indicating the squats depth was above 1.1 mm.

Overall, during approximately 2.5 years, the squats had considerably grown from small black spots without cracks to mature squats with widths of about 50 mm, surface depths up to 100 μm, and crack depths exceeding 1.1 mm. This result highlights the importance and urgency of addressing rail corrugation to prevent rapid RCF crack development and the potential catastrophic rail breaks.

5. Discussions

This section further interprets the numerical results and field observations and identifies the long-term evolution process of rail roughness and corrugation on this basis. Then, a widely reported hypothesis for corrugation formation, the so-called pinned-pinned resonance in the literature, is examined with some field observations.

5.1. Evolution of rail roughness and corrugation

Based on field observations and numerical simulations, the evolution of rail roughness is identified as a typical 'bathtub' curve, see a schematic drawing in Fig. 15a. This process can be divided into three phases: smoothing (I), stability (II) and degradation (III).

In Phase I, the initial rail roughness from manufacturing or maintenance like rail grinding is worn off and the rail surface becomes smoother. This is supported by the field measurement data (e.g., Fig. 8 and TU108 in Fig. 15b) and numerical simulations [32], which show that artificial marks are erased by the wheel-rail dynamic interaction and the resulting differential wear. Similar field observations have been reported in [50,60]. In Phrase II, the rail roughness overall stays a relatively low and stable level, and the rail is approximately evenly worn. During this phase, the eigenmodes of the vehicle-track system, such as vertical and lateral pinned-pinned modes, and longitudinal compression modes, should also be excited by the rail roughness, causing dynamic forces in three directions [37]. However, in nominal track conditions without initial excitation, none of these modes is dominant enough to induce differential wear or plastic deformation for corrugation formation [33]. Consequently, the resulting wear is approximately even on the rail surface under the superposition of dynamic forces in three directions, and the rail roughness remains stable. One example is present at TU072 on Track 3 where rail roughness barely changed after two years of service. Similar field observations have been reported in [18,60]. In Phrase III, rail roughness increases significantly due to the development of rail defects, such as corrugations and RCF, see one example at TU188 in Fig. 15d. Corrugations mainly occur in this phase because of the track degradation after a period of service, introducing initial excitations to the vehicle-track systems. Similar field observations have been widely reported in literature, such as in [18].

The bathtub curve in Fig. 15a qualitatively describes a typical evolution process of rail roughness, where Phases I and II represent nominal track conditions without initial excitation. In practice, initial excitation can also be introduced to the vehicle-track system at a very early stage caused by design and construction. For example, it was reported in [61] that the Vancouver mass transit system experienced severe corrugation

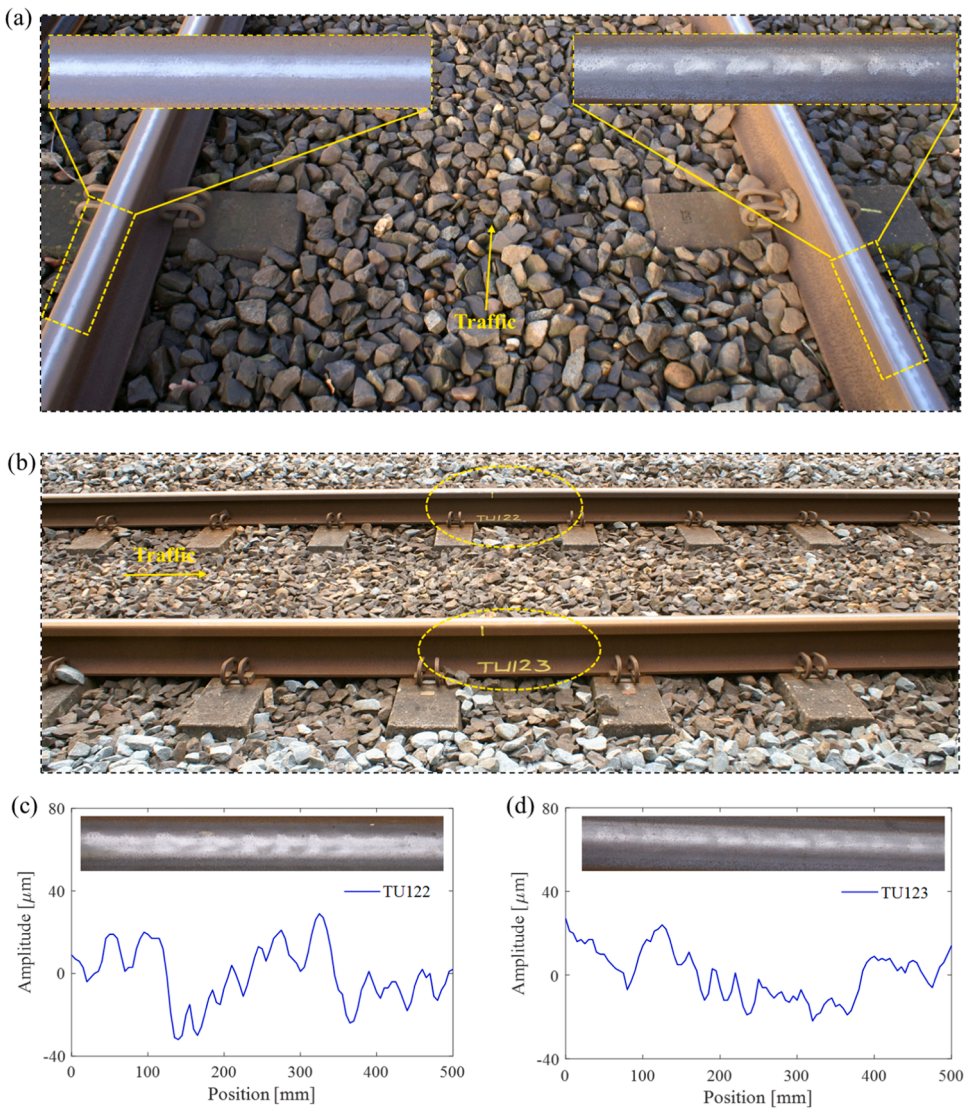

Fig. 13. Corrugation on the left and right rails. (a) One corrugation site on Track 1 at Steenwijk, and corrugation occurs on the right rail only; (b) TU122 and TU123 on Track 1 at Steenwijk, and corrugation occurs on both rails with different features; (c) the corrugation geometry at TU122; (d) the corrugation geometry at TU123.

shortly after opening due to the narrow track gauge that caused close conformity between the rail and the wheel and led to stick-slip oscillations. The phenomenon in the Beijing metro lines [62] indicate inappropriate rail fastening types also contributed to the fast growth of rail corrugation within a few months. The evolution tendency of rail roughness in these cases is illustrated as the red line in Fig. 15a, where initial excitation is introduced from the beginning of the operation.

In Phase III, due to the considerable increase in rail roughness, grinding activities often need to be arranged to improve the rail geometry, reduce the vibration and noise, and remove the initiation of rolling contact fatigue cracks. These benefits of grinding were confirmed in field observations. However, field data also show that corrugation rapidly reoccurs with the same wavelengths at the same location after grinding, as depicted by the green lines in Fig. 15a. Therefore, inadequate rail grinding acts more as a palliative measure rather than a cure for corrugation. The fundamental solution to corrugation is to improve the track dynamic behaviours to mitigate or eliminate initial excitation, such as, from Phase III to Phase II.

5.2. *Vertical pinned-pinned resonance cannot fully explain the corrugation*

Pinned-pinned resonance is a vertical rail bending mode whose wavelength is twice the sleeper spacing, and the modal frequency is primarily determined by rail bending stiffness and sleeper spacing. In the four monitored tracks with a nominal UIC54 rail profile and sleeper span of 0.6 m, the pinned-pinned resonance is approximately 1000–1100 Hz, as marked by the green circles in Fig. 16. The frequency is slightly higher at on-support than mid-span because of the additional support stiffness from fastenings and sleepers.

It is widely reported in the literature that vertical pinned-pinned resonance is the wavelength-fixing mechanism of short pitch corrugation [17,18,25,63], which is called ‘pinned-pinned resonance’ corrugation in [54]. The vertical pinned-pinned resonance has difficulty in explaining the following field observations on corrugation.

1. Corrugation does not occur everywhere but pinned-pinned resonance is everywhere on the discretely-supported tracks. All rails will eventually be corrugated according to the pinned-pinned resonance hypothesis. However, the field observations in this work and in [18, 53] indicate that some rails with pinned-pinned resonance remained

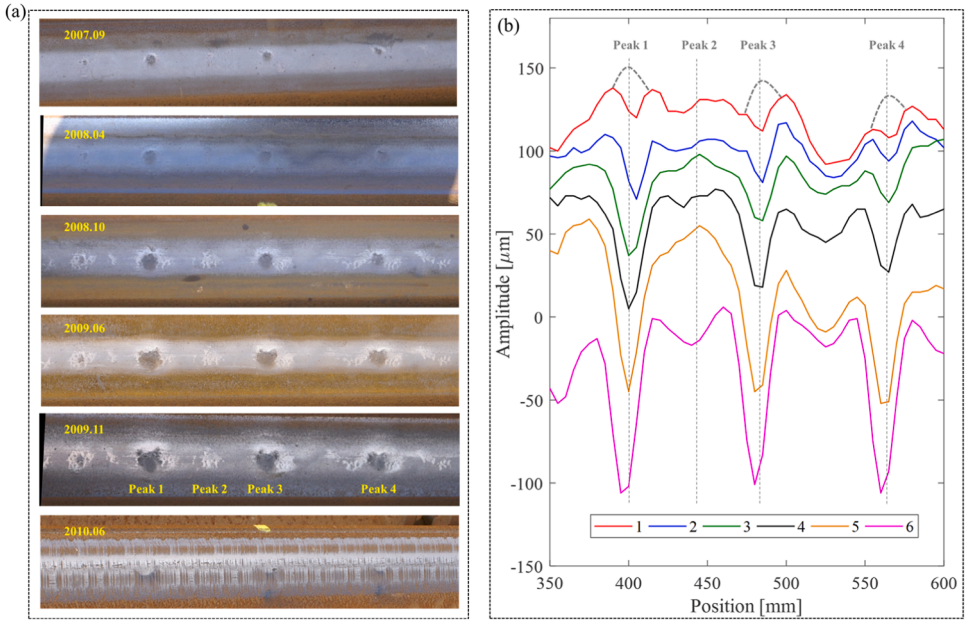

Fig. 14. The development of corrugation-induced squats. (a) corrugation-induced squats at TU109 on Track 1 during the first six observations; (b) the measured rail longitudinal-vertical profiles.

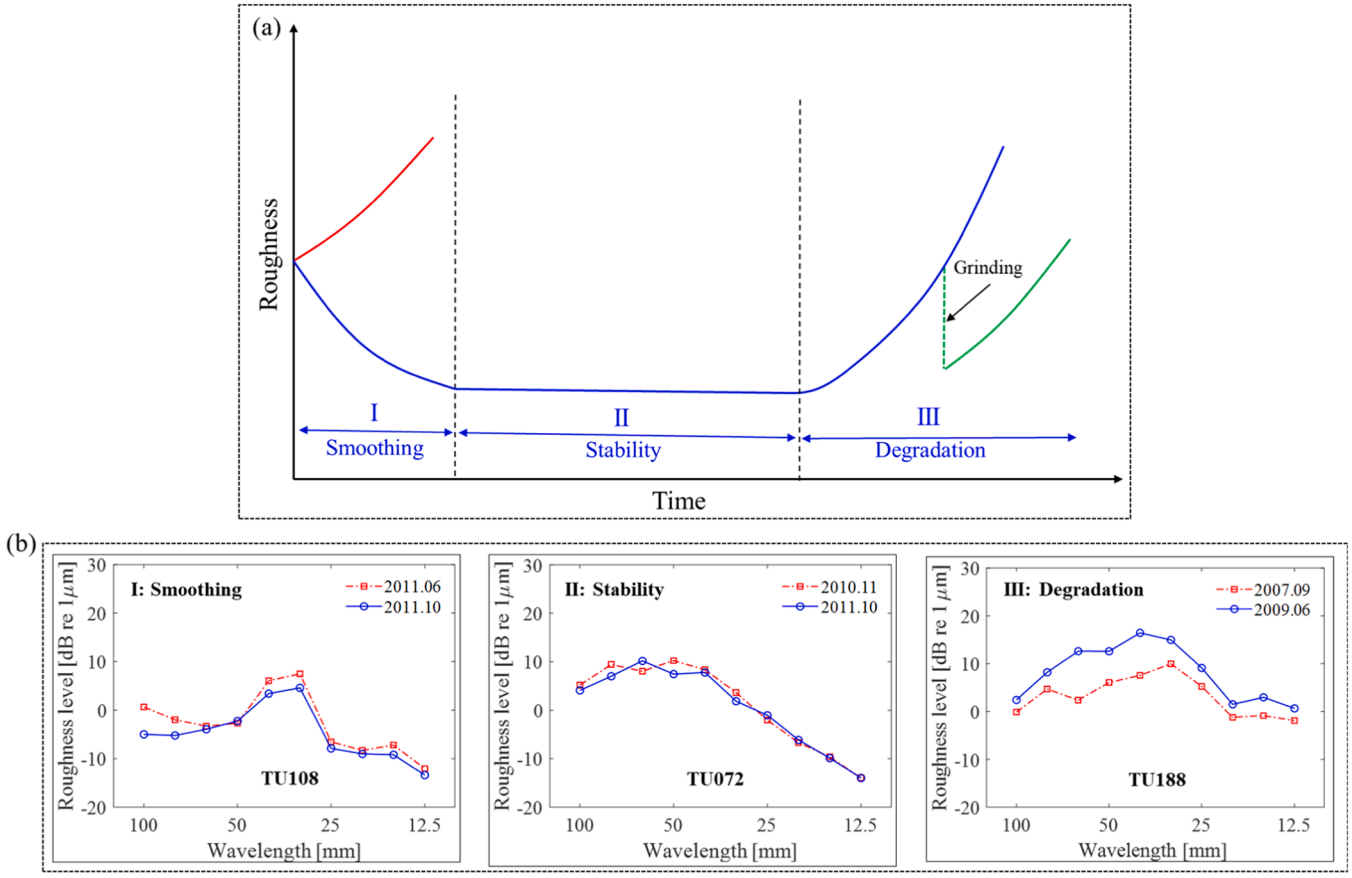

Fig. 15. The evolution of rail roughness. (a) a schematic drawing of rail roughness evolution in three phases: smoothing, stability and degradation; (b) examples of rail roughness evolution in the three phases.

corrugation-free after about 20 years of service in the Dutch railways.

2. With a traffic speed of 130–140 km/h in the four monitored tracks, pinned-pinned resonance could mainly influence the corrugation wavelengths at around 30–40 mm, which affects about 45 %, 32 %, 21 %, 18 % of corrugation wavelengths on the four tracks, respectively, as shown in Fig. 10. The other wavelength components cannot be explained by pinned-pinned resonance.

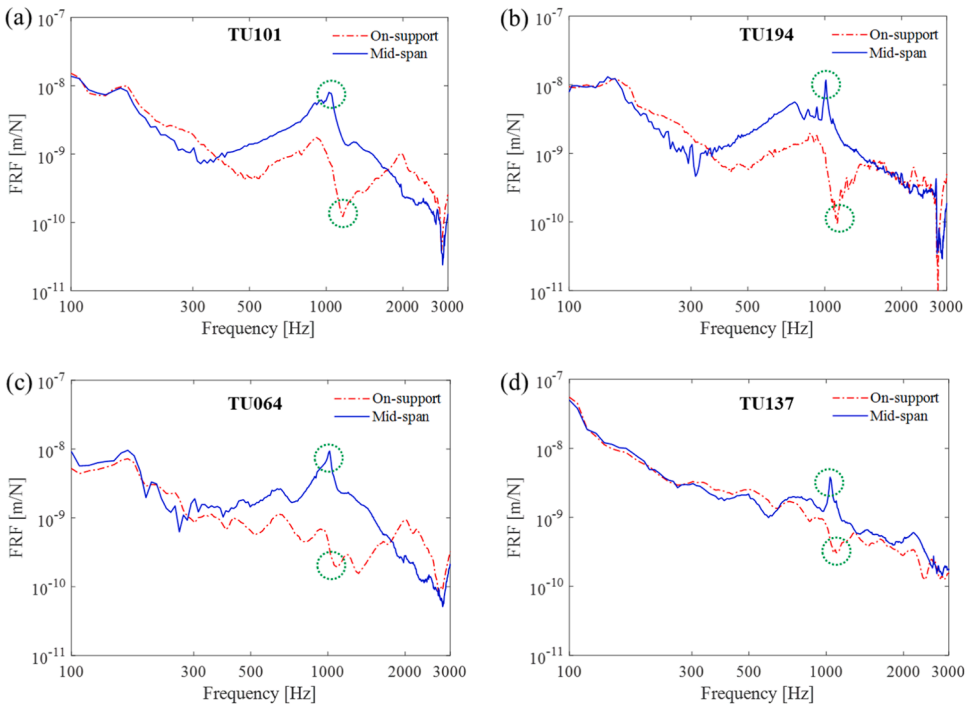

Fig. 16. The vertical FRFs of four monitored tracks in the Dutch railway. (a) TU101 on Track 1 at Steenwijk; (b) TU194 on Track 2 at Assen; (c) TU064 on Track 3 at Weert; (d) TU137 on Track 4 at Wirdum.

3. The grinding marks with the 35 mm wavelength, which excited the pinned-pinned resonance at a speed of 130 km/h, were worn off, as shown in Fig. 12b. This result indicates that the hypothesis may not hold, which assumes corrugation develops from pinned-pinned resonance excited by initial rail roughness.
4. Corrugation has been observed on embedded rail systems where pinned-pinned resonance is absent [4].

These field observations have been well explained by the numerical simulations in [32,33,36]. Future research could be performed to better understand the conditions under which the pinned–pinned resonance may effectively be triggered to induce corrugation.

6. Conclusions

This paper investigates the development mechanism of short pitch corrugation based on extensive field observations of 105 corrugations over a five-year period. Comprehensive field data were obtained during the eleven observations, including corrugation photos, geometry, track dynamic behaviours and vehicle-track dynamic responses.

The numerical predictions of the corrugation development process in [32,33,36] are validated by the field observations and measurements. It confirms that initial excitation is necessary for corrugation formation. Artificial corrugation from rail grinding marks was erased by wheel-rail rolling contact. Corrugation initiates and consistently grows at fixed locations with the continuous accumulation of differential wear, and will eventually reach a limiting amplitude. Rail longitudinal vibration modes and longitudinal wheel-rail vibration are crucial to corrugation initiation, while vertical vibration plays an increasingly important role during corrugation growth. Longitudinal vibration of shorter wavelengths might be inherently stronger in comparison to vertical vibration; which could set the upper bound of the corrugation wavelength, and the contact filter effect probably sets the lower bound. According to these observations and simulations, the evolution process of rail roughness is identified as a typical 'bathtub' curve, including three phases of smoothing, stability and degradation.

Based on the identified corrugation mechanism, the fundamental solution to corrugation is to improve the track dynamics by strengthening the rail longitudinal constraints, which can effectively suppress rail longitudinal vibration modes and mitigate corrugation initiation. Furthermore, the early detection or prediction of corrugation can be achieved based on the measurement of vehicle-track longitudinal dynamic response (e.g., longitudinal ABA) because of its significant role in corrugation initiation. In future work, further research could be performed to examine whether the proposed corrugation mechanism and mitigation approaches can be extended to explain and treat corrugation in other types of railway lines, such as high-speed or metro lines.

Statement of originality

As the corresponding author, I Pan Zhang, hereby confirm on behalf of all authors that:

1) The paper has not been published previously, that it is not under consideration for publication elsewhere, and that if accepted it will not be published elsewhere in the same form, in English or in any other language, without the written consent of the publisher.
2) The paper does not contain material which has been published previously, by the current authors or by others, of which the source is not explicitly cited in the paper.

CRediT authorship contribution statement

Zili Li: Writing – review & editing, Supervision, Resources, Project administration, Investigation, Funding acquisition, Formal analysis, Conceptualization. **Pan Zhang:** Writing – original draft, Visualization, Software, Methodology, Investigation, Formal analysis, Data curation, Conceptualization.

Declaration of Competing Interest

The authors declare that they have no known competing financial interests or personal relationships that could have appeared to influence the work reported in this paper.

Acknowledgements

The authors thank Dr. Shaoguang Li for helping with hammer tests and data acquisition in Zoetermeer, the Netherlands, in November 2023.

Data availability

Data will be made available on request.

References

[1] Mei G, Chen G. Slip of wheels on rails: the root cause for rail undulant wear. Wear 2023;523:204727.
[2] Torstensson P, Nielsen JC. Monitoring of rail corrugation growth due to irregular wear on a railway metro curve. Wear 2009;267:556–61.
[3] Correa N, Oyarzabal O, Vadillo E, Santamaria J, Gomez J. Rail corrugation development in high speed lines. Wear 2011;271:2438–47.
[4] Oostermeijer K. Review on short pitch rail corrugation studies. Wear 2008;265:1231–7.
[5] Grassie S, Kalousek J. Rail corrugation: characteristics, causes and treatments. Proc Inst Mech Eng, Part F J Rail Rapid Transit 1993;207:57–68.
[6] Wei Z, Sun X, Yang F, Ke Z, Lu T, Zhang P, et al. Carriage interior noise-based inspection for rail corrugation on high-speed railway track. Appl Acoust 2022;196:108881.
[7] Thompson D. Wheel-rail noise generation, part IV: contact zone and results. J Sound Vib 1993;161:447–66.
[8] Zhao X, Yang J, An B, Liu C, Cao Y, Wen Z, et al. Determination of dynamic amplification factors for heavy haul railways. Proc Inst Mech Eng, Part F J Rail Rapid Transit 2018;232:514–28.
[9] Deng X, Qian Z, Li Z, Dollevoet R. Investigation of the formation of corrugation-induced rail squats based on extensive field monitoring. Int J Fatigue 2018;112:94–105.
[10] Kaewunruen S, Ngamkhanong C, Lim CH. Damage and failure modes of railway prestressed concrete sleepers with holes/web openings subject to impact loading conditions. Eng Struct 2018;176:840–8.
[11] Wang P, Lu J, Zhao C, Chen M, Xing M. Numerical investigation of the fatigue performance of elastic rail clips considering rail corrugation and dynamic axle load. Proc Inst Mech Eng, Part F J Rail Rapid Transit 2021;235:339–52.
[12] Wei L, Sun Y, Zeng J, Qu S. Experimental and numerical investigation of fatigue failure for metro bogie cowcatchers due to modal vibration and stress induced by rail corrugation. Eng Fail Anal 2022;142:106810.
[13] Gray G, Johnson K. The dynamic response of elastic bodies in rolling contact to random roughness of their surfaces. J Sound Vib 1972;22:323–42.
[14] Zhai W, Wang K, Cai C. Fundamentals of vehicle–track coupled dynamics. Veh Syst Dyn 2009;47:1349–76.
[15] Zhao X, Zhang P, Wen Z. On the coupling of the vertical, lateral and longitudinal wheel-rail interactions at high frequencies and the resulting irregular wear. Wear 2019;430:317–26.
[16] Zhang P, He C, Shen C, Dollevoet R, Li Z. Comprehensive validation of three-dimensional finite element modelling of wheel-rail high-frequency interaction via the V-Track test rig. Veh Syst Dyn 2024:1–25.
[17] Hempelmann K, Knothe K. An extended linear model for the prediction of short pitch corrugation. Wear 1996;191:161–9.
[18] Hiensch M, Nielsen JC, Verheijen E. Rail corrugation in the Netherlands—measurements and simulations. Wear 2002;253:140–9.
[19] Li W, Zhou Z, Zhao X, Wen Z, Jin X. Formation mechanism of short-pitch rail corrugation on metro tangent tracks with resilient fasteners. Veh Syst Dyn 2022:1–24.
[20] Gómez I, Vadillo E. A linear model to explain short pitch corrugation on rails. Wear 2003;255:1127–42.
[21] Robles R, Correa N, Vadillo EG, Blanco-Lorenzo J. Comprehensive efficient vertical and lateral track dynamic model to study the evolution of rail corrugation in sharp curves. J Sound Vib 2023;545:117448.
[22] Wu T, Thompson D. An investigation into rail corrugation due to micro-slip under multiple wheel/rail interactions. Wear 2005;258:1115–25.
[23] Johansson A, Nielsen JC. Rail corrugation growth—influence of powered wheelsets with wheel tread irregularities. Wear 2007;262:1296–307.
[24] Ma C, Gao L, Xin T, Cai X, Nadakatti MM, Wang P. The dynamic resonance under multiple flexible wheelset-rail interactions and its influence on rail corrugation for high-speed railway. J Sound Vib 2021;498:115968.
[25] Muller S. A linear wheel–track model to predict instability and short pitch corrugation. J Sound Vib 1999;227:899–913.
[26] Knothe K, Groß-Thebing A. Short wavelength rail corrugation and non-steady-state contact mechanics. Veh Syst Dyn 2008;46:49–66.
[27] Cui X, Chen G, Yang H, Zhang Q, Ouyang H, Zhu M. Study on rail corrugation of a metro tangential track with Cologne-egg type fasteners. Veh Syst Dyn 2016;54:353–69.
[28] Grassie SL, Edwards JW. Development of corrugation as a result of varying normal load. Wear 2008;265:1150–5.
[29] Zhao X, Li Z, Dollevoet R. The vertical and the longitudinal dynamic responses of the vehicle–track system to squat-type short wavelength irregularity. Veh Syst Dyn 2013;51:1918–37.
[30] Grassie S, Gregory R, Johnson K. The dynamic response of railway track to high frequency longitudinal excitation. J Mech Eng Sci 1982;24:97–102.
[31] Li Z, Molodova M, Núñez A, Dollevoet R. Improvements in axle box acceleration measurements for the detection of light squats in railway infrastructure. IEEE Trans Ind Electron 2015;62:4385–97.
[32] Li S, Li Z, Núñez A, Dollevoet R. New insights into the short pitch corrugation enigma based on 3D-FE coupled dynamic vehicle-track modeling of frictional rolling contact. Appl Sci 2017;7:807.
[33] Li Z, Li S, Zhang P, Núñez A, Dollevoet R. Mechanism of short pitch rail corrugation: initial excitation and frequency selection for consistent initiation and growth. Int J Rail Transp 2022:1–36.
[34] Zhang P, Li S, Li Z. Short pitch corrugation mitigation by rail constraint design. Int J Mech Sci 2022:108037.
[35] Zhang P, Li Z. Experimental study on the development mechanism of short pitch corrugation using a downscale V-Track test rig. Tribology Int 2023:108293.
[36] Zhang P, Li S, Dollevoet R, Li Z. Parametric investigation of railway fastenings into the formation and mitigation of short pitch corrugation. Railw Eng Sci 2024.
[37] Zhang P, Li Z. New experimental evidences of corrugation formation due to rail longitudinal vibration mode. Int J Rail Transp 2024:1–22.
[38] Yang Z, Deng X, Li Z. Numerical modeling of dynamic frictional rolling contact with an explicit finite element method. Tribology Int 2019;129:214–31.
[39] Naeimi M, Li Z, Petrov RH, Sietsma J, Dollevoet R. Development of a new downscale setup for wheel-rail contact experiments under impact loading conditions. Exp Tech 2018;42:1–17.
[40] Vo K, Tieu AK, Zhu H, Kosasih PB. A 3D dynamic model to investigate wheel–rail contact under high and low adhesion. Int J Mech Sci 2014;85:63–75.
[41] Xu L, Chen X, Li X, He X. Development of a railway wagon-track interaction model: case studies on excited tracks. Mech Syst Signal Process 2018;100:877–98.
[42] Shen C, Deng X, Wei Z, Dollevoet R, Zoeteman A, Li Z. Comparisons between beam and continuum models for modelling wheel-rail impact at a singular rail surface defect. Int J Mech Sci 2021;198:106400.
[43] Suda Y, Komine H, Iwasa T, Terumichi Y. Experimental study on mechanism of rail corrugation using corrugation simulator. Wear 2002;253:162–71.
[44] Jin X, Wen Z. Rail corrugation formation studied with a full-scale test facility and numerical analysis. Proc Inst Mech Eng, Part J J Eng Tribology 2007;221:675–98.
[45] Bellette P, Meehan P, Daniel W. Validation of a tangent track corrugation model with a two disk test rig. Wear 2011;271:268–77.
[46] Zhao X, Li Z. The solution of frictional wheel–rail rolling contact with a 3D transient finite element model: validation and error analysis. Wear 2011;271:444–52.
[47] Molodova M, Li Z, Núñez A, Dollevoet R. Validation of a finite element model for axle box acceleration at squats in the high frequency range. Comput Struct 2014;141:84–93.
[48] Oregui M, Li Z, Dollevoet R. An investigation into the modeling of railway fastening. Int J Mech Sci 2015;92:1–11.
[49] Yang Z, Li Z. A numerical study on waves induced by wheel-rail contact. Int J Mech Sci 2019;161:105069.
[50] Grassie SL. Short wavelength rail corrugation: field trials and measuring technology. Wear 1996;191:149–60.
[51] Li Z, Dollevoet R, Molodova M, Zhao X. Squat growth—some observations and the validation of numerical predictions. Wear 2011;271:148–57.
[52] Oregui M, Molodova M, Núñez A, Dollevoet R, Li Z. Experimental investigation into the condition of insulated rail joints by impact excitation. Exp Mech 2015;55:1597–612.
[53] Dings P, Dittrich M. Roughness on Dutch railway wheels and rails. J Sound Vib 1996;193:103–12.
[54] Grassie S. Rail corrugation: characteristics, causes, and treatments. Proc Inst Mech Eng, Part F J Rail Rapid Transit 2009;223:581–96.
[55] Zhang P, Li S, Núñez A, Li Z. Vibration modes and wave propagation of the rail under fastening constraint. Mech Syst Signal Process 2021;160:107933.
[56] Vernaillen T, Wang L, Núñez A, Dollevoet R, Li Z. Rail wear rate on the Belgian railway network–a big-data analysis. Int J Rail Transp 2023:1–16.
[57] Afferrante L, Ciavarella M. Short pitch corrugation of railway tracks with wooden or concrete sleepers: an enigma solved? Tribology Int 2010;43:610–22.
[58] Du X, Jin X, Zhao G, Wen Z, Li W. Rail corrugation of high-speed railway induced by rail grinding. Shock Vib 2021;2021:1–14.
[59] Li S, Naeimi M, He C, Dollevoet R, Li Z. An integrated 3D dynamic FE vehicle-track model in elasto-plasticity to investigate short pitch corrugation under cyclic wheel loads. Struct Elsevier 2023:1000–11.
[60] Croft B.E., The development of rail-head acoustic roughness: University of Southampton; 2009.
[61] Kalousek J, Johnson K. An investigation of short pitch wheel and rail corrugations on the Vancouver mass transit system. Proc Inst Mech Eng, Part F J Rail Rapid Transit 1992;206:127–35.
[62] Liu W, Zhang H, Liu W, Thompson DJ. Experimental study of the treatment measures for rail corrugation on tracks with Egg fasteners in the Beijing metro. Proc Inst Mech Eng, Part F J Rail Rapid Transit 2018;232:1360–74.
[63] Nielsen J. Numerical prediction of rail roughness growth on tangent railway tracks. J Sound Vib 2003;267:537–48.